Acta Cryst. (1996). A52, 923–936

Low-Order Structure-Factor Amplitude and Sign Determination of an Unknown Structure Al_mFe by Quantitative Convergent-Beam Electron Diffraction

Y. F. CHENG,[a]*† W. NÜCHTER,[a] J. MAYER,[a] A. WEICKENMEIER[a] AND J. GJØNNES[b]

[a]*Max-Planck-Institut für Metallforschung, Institut für Werkstoffwissenschaft, Seestrasse 92, 70174 Stuttgart, Germany, and* [b]*Center for Materials Research, University of Oslo, Gaustadallèen 21, 0371 Oslo, Norway. E-mail: ycheng@sb.fsu.edu*

(Received 28 December 1995; accepted 24 June 1996)

Abstract

An iterative method for the determination of structure-factor amplitudes and phases of crystals with unknown structure is proposed. The method is based on the quantitative evaluation of energy-filtered convergent-beam electron diffraction (CBED) patterns. It has been applied to the metastable phase Al_mFe ($m = 4.2$–4.4), which was found as primary particles in commercial aluminium alloys. When the rocking curves of reflections along a (100) systematic row are fitted, a number of structure-factor amplitudes and signs of $h00$-type reflections of Al_mFe have been determined successfully. The accuracy of the structure-factor amplitudes is better than 5% for the strong reflections and about 10% for the weak reflections. The aim of this method is to provide accurate structure-factor data, including both amplitudes and phases, for *ab initio* structure determination and refinement of unknown structures by using electron diffraction techniques.

1. Introduction

Crystallographic methods for structure determination are commonly based on diffraction experiments, in which the intensities of the diffracted beams rather than the structure factors are measured. If the kinematical scattering approximation is valid, like in an X-ray or a neutron diffraction experiment, a linear relationship exists between the diffraction intensities and the square of the structure-factor amplitudes but the phases of the structure factors are lost. For X-ray or neutron diffraction, very successful structure determination techniques, based on Patterson maps (see, for instance, Giacovazzo, 1992) or the direct phasing method (Woolfson, 1961), have already been developed. There exist standardized routines covering each single step from experimental data collection to locating atoms within the unit cell of a crystal with an unknown structure. But no such routine exists in electron diffraction, although structure determination and refinement from electron diffraction may be a practical alternative when suitable samples for X-ray and neutron diffraction are not available. Therefore, for a long time, it has been a task for many electron crystallographers to solve unknown crystal structures solely by electron-microscopy techniques, *i.e. ab initio* structure determination.

The minimum requirement for structure determination from electron diffraction is a sufficient set of kinematical, or near kinematical, intensities measured with satisfactory accuracy. These kinematical intensity data could then be treated by standard methods known from X-ray crystallography. Analysis of experimental electron diffraction intensity data along such lines has been applied successfully to organic crystals (Dorset, 1991) and even to some inorganic materials under conditions when kinematical scattering is predominant. Unfortunately, this is not the case for most inorganic materials.

In the case of dynamical scattering, there is no simple relationship between the structure-factor amplitudes and the intensities of the corresponding diffracted beams. In addition to the dynamical effects, the intensities of conventional selected-area electron diffraction patterns are affected by different excitation errors. Furthermore, the intensities are averaged over an illuminated crystal area whose thickness may vary in an unspecified way. Hence, in electron diffraction the spot pattern intensities are much less useful than the integrated intensities obtained by X-ray and neutron diffraction. Up to now, the usual way to overcome the problem of dynamical effects has been to reduce the effects by using a thin crystal or stick to structures with only light atoms. Another possibility is to use the intensities of high-order reflections whose extinction distances are longer than those of the low-order reflections and therefore are less affected by the dynamical effects (Taftø & Metzger, 1985). The convergent-beam electron diffraction (CBED) technique, on the other hand, offers the possibility of collecting the integrated intensities. Taftø & Metzger (1985) proposed a method for the intensity measure-

† Present address: Institute of Molecular Biophysics, Florida State University, Tallahassee, Florida 32306-3015, USA.

ment of high-order reflections along a systematic row, where the integrated intensities could be treated kinematically. An application of this technique to a structure refinement has been described by Ma, Romming, Lebech, Gjønnes & Taftø (1992). Vincent & Bird (1986) developed another method for the kinematic intensity measurement of high-order Laue-zone (HOLZ) reflections and determined the structure of a metastable Al–Ge phase (Vincent & Exelby, 1995). A precession electron diffraction technique developed by Vincent & Midgley (1994) offers the possibility of collecting a large diffraction data set of integrated intensity. A structure determination of the rare-earth pyrogermanate $Er_2Ge_2O_7$ was successfully performed by using the diffraction data set of high-order reflections obtained by this technique (Midgley, Sleight & Vincent, 1994).

Dynamical scattering makes direct analysis of the diffraction intensities difficult but, in turn, it provides the possibility of determining the phases of the structure factors. Several quantitative CBED techniques have been developed by different groups for the purpose of determination of accurate structure-factor amplitudes and phases of crystals whose structures are already known (Zuo, Spence & O'Keeffe, 1988; Bird & Saunders, 1992; Holmestad, Zuo, Spence, Høier & Horita, 1995). The quantitative technique developed by Zuo & Spence (1991) is for automated structure-factor amplitude and phase refinement from CBED patterns. It uses a many-beam dynamical calculation for the rocking-curve fitting. The structure factors of the reflections that satisfy the Bragg condition along a systematic row are refined during the rocking-curve fitting. This technique has been modified by Deininger, Necker & Mayer (1994), who improved the refinement process by utilizing a global refinement algorithm, and by Nüchter, Weickenmeier & Mayer (1995). The structure-factor amplitudes and phases obtained by these techniques are accurate enough to provide information on the bonding charge distribution of crystals. However, the method has never been used for structure determination of unknown crystal structures.

In the present investigation, we have, for the first time, applied the quantitative CBED technique to a crystal of unknown structure in order to determine accurate structure-factor amplitudes *and* phases. A series of structure-factor amplitudes and signs of the reflections along a systematic row have been determined successfully. The experimental accuracies and limitations will be discussed. The accurate structure factors determined with our new method, which in the given case cannot be obtained by any other technique, are an important step forward in the effort towards *ab initio* structure determination from electron diffraction techniques.

2. Material and experiment

2.1. *Al_mFe: an unknown phase*

The metastable phase Al_mFe ($m = 4.2$–4.4) is commonly observed as primary particles in commercial aluminium alloys cast with high cooling rates. Its unit cell is body-centered tetragonal with $a = 8.84$, $c = 21.6$ Å (Miki, Kosuge & Nagahama, 1975). The space group has been reported to be $I4/mmm$ (No. 139), a centrosymmetrical space group, by Skjerpe, Gjønnes & Langsrud (1987) and Cheng, Hui & Li (1991) from its selected-area electron diffraction patterns and CBED patterns. In this space group, a structure model with Fe surrounded by Al in a CsCl-type local arrangement as a building block has been proposed by Skjerpe (1988). The model contains about 110 atoms (90 Al and 20 Fe). No refinement was attempted for this structure model, which thus must be regarded as tentative.

Owing to the centrosymmetric of the $I4/mmm$ space group, the phases of all its structure factors are either 0 or π. However, it should be noted that another space group, $I\bar{4}m2$ (No. 121), which is a non-centrosymmetric space group, was suggested by Hansen, Berg & Gjønnes (1995). The Patterson sections calculated from the precession electron diffraction data of the Al_mFe phase are incompatible with the $4mm$ symmetry along the [001] zone axis but correspond to a $\bar{4}m2$ symmetry. However, even for the non-centrosymmetric space group $I\bar{4}m2$, the structure-factor phases of the $hk0$ reflections remain either 0 or π because of the (110) mirror plane.

2.2. *Experiment*

The powder sample of Al_mFe was prepared from the commercial twin-roll cast AA5052 [Al–2.5%Mg–0.24%Cr–0.28%Fe–0.05%Si (wt%)] alloy by using an extraction technique described by Simensen, Fartum & Anderson (1984) and Strid & Simensen (1986). The

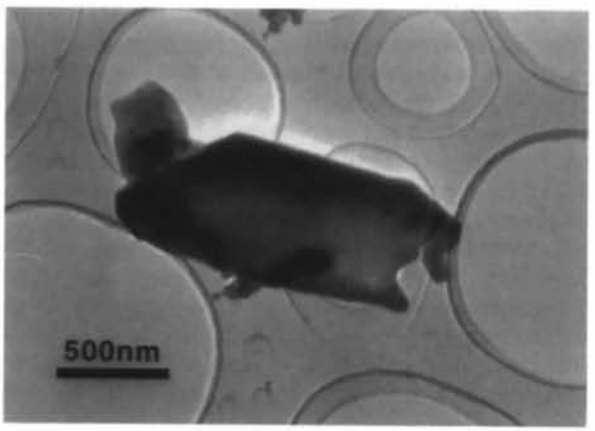

Fig. 1. Bright-field image of a single-crystal Al_mFe particle on the holey carbon film.

strip cast aluminium alloy that contains the Al_mFe phase as primary particles was dissolved in butanol. Extracted crystals, which are suitable for the TEM observation, were collected with a filter. The TEM samples were then prepared by dispersing the crystals in alcohol and collecting them on holey carbon grids. The particles of Al_mFe are in the size range 1–10 μm. Fig. 1 shows a bright-field image of such a particle. The Al_mFe particles are usually single crystals but often with a complicated morphology.

A Zeiss EM 912 Omega Energy Filtering Transmission Electron Microscope was used for the CBED experiments. The microscope is equipped with an LaB_6 filament and was operated at 120 kV. The novel built-in imaging Omega energy filter removes the electrons that have suffered inelastic scattering. In the energy-dispersive plane of the filter, the slit was adjusted to yield an energy width of 10 eV, which is sufficient to remove most of the inelastically scattered electrons. A Gatan double-tilt liquid-nitrogen-cooled specimen holder was used in order to reduce the contamination by the illuminating beam and to minimize the thermal diffuse scattering that cannot be removed by the energy filter. The specimens were cooled to nominal temperatures of 110–120 K and the total probe current was kept so that the estimated beam heating in the irradiated area did not exceed 10 K. The probe size used was about 20 nm. All energy-filtered CBED patterns were acquired directly with a Gatan 1024 × 1024 pixel slow-scan CCD camera attached to the Zeiss microscope and operated with the Gatan Digital Micrograph software. The digitized CBED patterns are then transferred to DEC3000 workstations for further processing.

2.3. *Data processing*

All CBED patterns were deconvoluted with the point-spread function of the CCD camera (Weickenmeier, Nüchter & Mayer, 1995) before any further processing. The crystal was tilted to an orientation in which only the reflections along a systematic row are strongly excited and the off-systematic-row reflections are as weak as possible. Then the intensity distribution inside the reflection discs shows characteristic fringes, which are called rocking-curve fringes. Line scans were extracted to obtain intensity profiles across the fringes.

In principle, the intensity distribution in any CBED pattern is determined by the structure factors (both elastic and inelastic structure factors) of the reflections, the thickness of the sample and the direction of the incident beam. The intensity distribution across the fringes is equivalent to rocking curves around the Bragg positions of systematic row reflections. An automated rocking-curve-fit program was used for structure-factor determination. The details of the program are described by Nüchter *et al.* (1995). The goodness of the fit is defined by a χ^2 criterion, where

$$\chi^2 = (1/N)\sum_{i=1}^{N}(cI_i^{\text{theo}} - I_i^{\text{exp}})^2/\sigma_i^2.$$

Here, I_i^{exp} and I_i^{theo} are the experimental and calculated intensity values of the point i within the line scan, c is a normalization constant and σ_i is standard deviation of experimental intensity in pixel i.

In addition to the structure factors and the thickness, there are four geometrical parameters that have to be refined in the process of rocking-curve fitting. There are two parameters for defining the incident-beam direction and two parameters for defining the length and the orientation of the reciprocal-lattice vector **g** in the diffraction pattern. Since only the reflections along the systematic row are included in the many-beam calculation, only one parameter defining the incident-beam direction has to be refined and the second one is always kept fixed. This parameter can be refined very accurately from the rocking-curve fitting. However, the length and orientation of the **g** vector are more flexible if only one line scan across the rocking-curve fringes is fitted, since both the length and the orientation could be changed simultaneously to fit the intensity profile, which in turn changes both the thickness and the structure-factor amplitude in the refinement. To overcome this problem, two parallel line scans were taken across each pattern. If the intensity profiles of the two line scans are fitted, the **g** vector orientation can be fixed. If two Bragg positions are present in one CBED pattern with systematic reflections, the length of the **g** vector can also be refined very accurately.

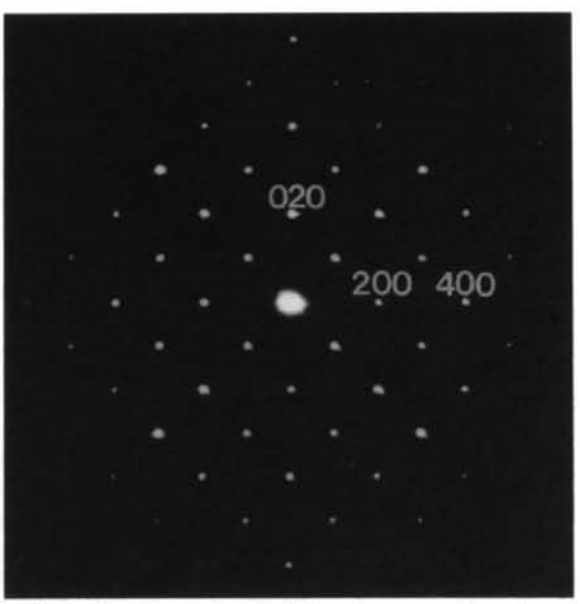

Fig. 2. A selected-area electron diffraction pattern taken along the [001] zone axis of the Al_mFe particle.

Table 1. $|U_{600}|$ *determined from two-beam rocking-curve fit*

No.	$\|U_{600}\|$ (Å^{-2})	ΔU_{600} (Å^{-2})	t (Å)	χ^2
1	0.016253	0.000052	1330	16.0
2	0.017033	0.000053	1545	13.3
3	0.016737	0.000085	1352	29.9
4	0.016733	0.000092	1117	8.4
Average	0.01669	0.00028		

Table 2. U_{200} *and* U_{400} *determined from four-beam calculation by setting* $U_{600} = +0.016\,69$ Å^{-2}

These structure factors correspond to two different local minima in the refinements.

No.	U_{200} (Å^{-2})	U_{400} (Å^{-2})	t (Å)	χ^2
1	−0.012285	+0.014289	1457	30.7
2	−0.012096	+0.014392	1527	22.8
3	−0.011701	+0.013536	1499	23.8
4	−0.012210	+0.014565	1214	20.0
5	−0.012608	+0.014693	1434	18.5
6	−0.012442	+0.014784	1719	24.6
Average	−0.01222 (28)	+0.01438 (41)		
No.	U_{200} (Å^{-2})	U_{400} (Å^{-2})	t (Å)	χ^2
1	+0.010700	+0.010548	1522	49.7
2	+0.011144	+0.012236	1537	21.6
3	+0.010757	+0.011656	1501	21.4
4	+0.011039	+0.012118	1239	21.6
5	+0.011379	+0.012348	1454	17.7
6	+0.011307	+0.012656	1719	24.4
Average	+0.01105 (25)	+0.01193 (68)		

3. Structure-factor determination

In the two-beam approximation, the structure-factor amplitude of the reflection in the Bragg condition can be directly determined from the positions of the rocking-curve fringes. However, the two-beam approximation is usually not sufficient for accurate determination of structure factors and it gives no information on the phase of the structure factor. If a many-beam calculation is used to determine an accurate structure factor by fitting the rocking curve, the structure factors of all other reflections involved in the calculation must be known, which is not the case of an unknown crystal structure. To overcome this problem, an iterative procedure is developed. The procedure starts with a two-beam structure-factor determination of one of the strong reflections along a systematic row and successively includes more beams along the systematic row. Here, as an example, the analysis of the (100) systematic row is described in detail.

Fig. 2 shows a selected-area electron diffraction pattern taken along the [001] zone axis of the Al_mFe phase. Along the (100) systematic row, the 600 reflection is the strongest reflection. CBED patterns were acquired in the systematic row orientation where only the $h00$ (h = even) reflections are strongly excited. Fig. 3(*a*) shows such a CBED pattern with the 600 reflection in the Bragg condition. The position of one line scan is indicated in the CBED pattern. The second line scan, which is not indicated in the CBED pattern, was made parallel to this one. The structure-factor amplitude of 600 was determined with the two-beam rocking-curve fit by adjusting both the structure-factor amplitude $|U_{600}|$ and the thickness t. Fig. 3(*b*) shows a two-beam rocking-curve fit. The circles in Fig. 3(*b*) represent the experimental intensity profile across the rocking-curve fringes of four reflection discs: 200, 400, 600 and 800, while the solid line is the calculated intensity profile. The lower part of Fig. 3(*b*) shows the differences between the calculated and experimental intensities at each pixel, where the definition of diff/sigma is $(cI_i^{\text{theo}} - I_i^{\text{exp}})/\sigma_i$. Only the rocking curve of 600 is fitted in the two-beam calculation. The structure-factor amplitude and thickness determined from this pattern are $|U_{600}| = 0.016\,253\,(52)$ Å^{-2} and $t = 1330$ Å. The χ^2 of the two-beam rocking-curve fit is 16.0. $|U_{600}|$ is determined in the two-beam approximation from four CBED patterns, which were acquired from specimen areas of different thickness and different orientation perpendicular to the (100) systematic row. Table 1 gives the results of the two-beam rocking-curve fit of all four patterns. The averaged two-beam structure-factor amplitude of 600 is $|U_{600}| = 0.016\,69\,(28)$ Å^{-2}.

Fig. 4(*a*) shows another CBED pattern where both the 200 and 400 reflections are on the Bragg positions. A four-beam (000, 200, 400, 600) calculation was then applied to fit the rocking curve of the discs 200, 400 and 600. U_{600} was set to be $+0.016\,69$ Å^{-2}, while U_{200} and U_{400} were refined together with the thickness t. Changing the sign of U_{600} corresponds to a shift of the origin in the unit cell, as will be discussed later. The refinement ranges of both U_{200} and U_{400} were set from a negative value to a positive value, which means that the signs of the structure factors are refined together with their value. Here, the positive sign corresponds to the phase of 0 and the negative sign to the phase of π. Two local minima with different χ^2 values were found in the refinement corresponding to different sign combinations of U_{200} and U_{400}. They are:

$$U_{200} = -0.012\,096\,(54)\,\text{Å}^{-2};$$
$$U_{400} = +0.014\,392\,(144)\,\text{Å}^{-2};$$
$$t = 1527\,\text{Å}; \quad \chi^2 = 22.8;$$

and

$$U_{200} = +0.011\,144\,(44)\,\text{Å}^{-2};$$
$$U_{400} = +0.012\,236\,(127)\,\text{Å}^{-2};$$
$$t = 1537\,\text{Å}; \quad \chi^2 = 21.6.$$

Fig. 4(*b*) shows a rocking-curve fit of this pattern, the corresponding χ^2 is 22.8. U_{200} and U_{400} were refined in the same way from six different CBED patterns, which

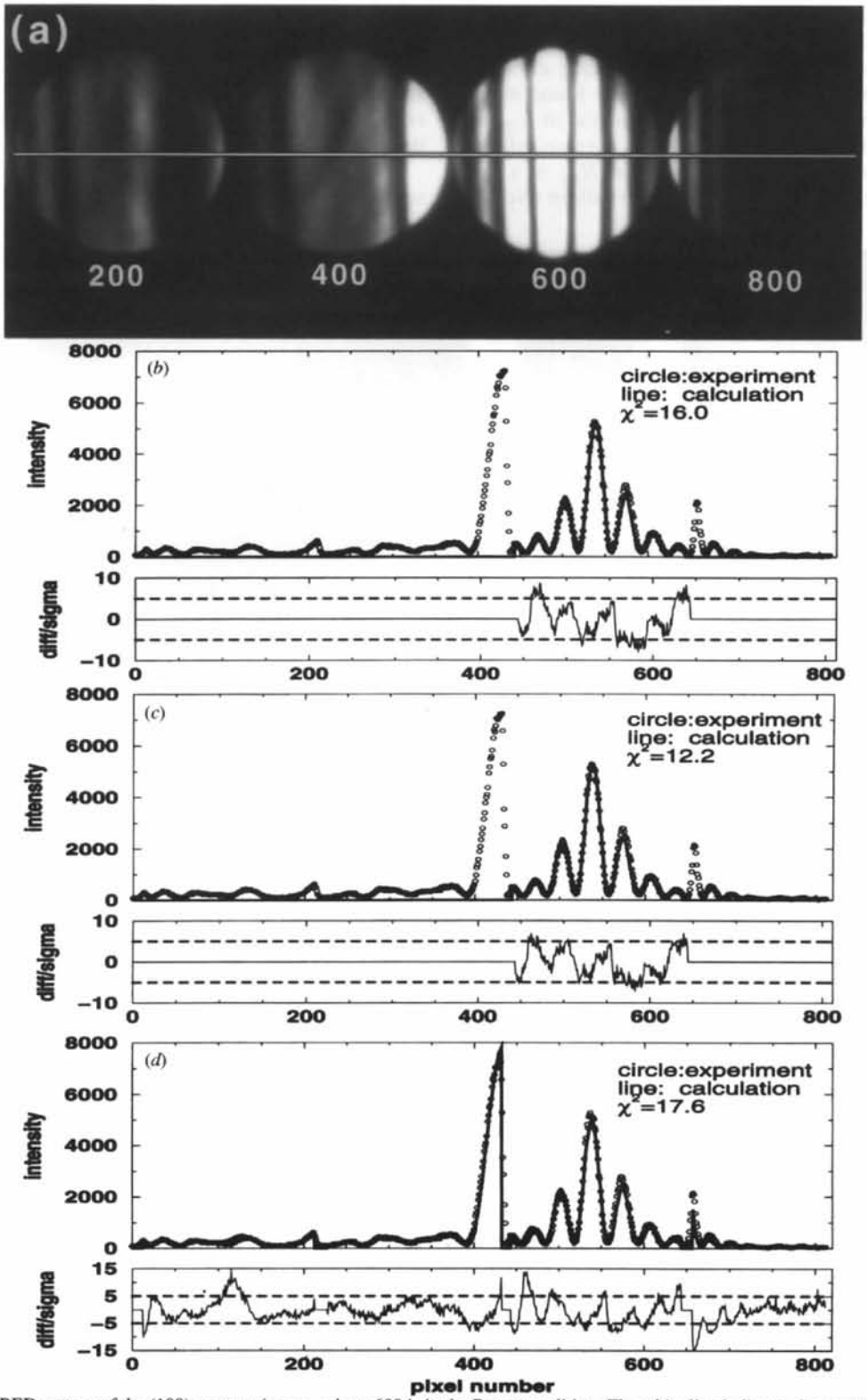

Fig. 3. (*a*) A CBED pattern of the (100) systematic row, where 600 is in the Bragg condition. The white line indicates the position of a line scan. (*b*) A two-beam rocking-curve fit for determining $|U_{600}|$. $|U_{600}| = 0.016\,253\,\text{Å}^{-2}$, $t = 1330\,\text{Å}$. (*c*) A four-beam (000, 200, 400, 600) rocking-curve fit for refining U_{600}: $U_{600} = +0.013\,222\,\text{Å}^{-2}$, $t = 1370\,\text{Å}$. (*d*) A 15-beam rocking-curve fit for refining U_{600}: $U_{600} = +0.012\,884\,\text{Å}^{-2}$, $t = 1330\,\text{Å}$.

were recorded from different Al_mFe particles of different thicknesses and are denoted hereafter as $g200$–$g400$ patterns. By fitting the rocking curves of all these patterns, two local minima were found in each of the refinements. A plot of χ^2 as a function of U_{200} and U_{400} (Fig. 5*a*) shows two local minima corresponding to different sign combinations of U_{200} and U_{400} in a four-beam rocking-curve fit of a $g200$–$g400$ pattern (No. 2 in Table 2). Table 2 gives the values of U_{200} and U_{400} that correspond to those two local minima refined from six different CBED patterns, its average value and the standard deviation. The difference of the χ^2 between the two local minima is not big enough to decide which of them corresponds to the right structure factors.

As the preliminary value of $U_{600} = +0.016\,98\,\text{Å}^{-2}$ was obtained as a 'two-beam structure factor', it is

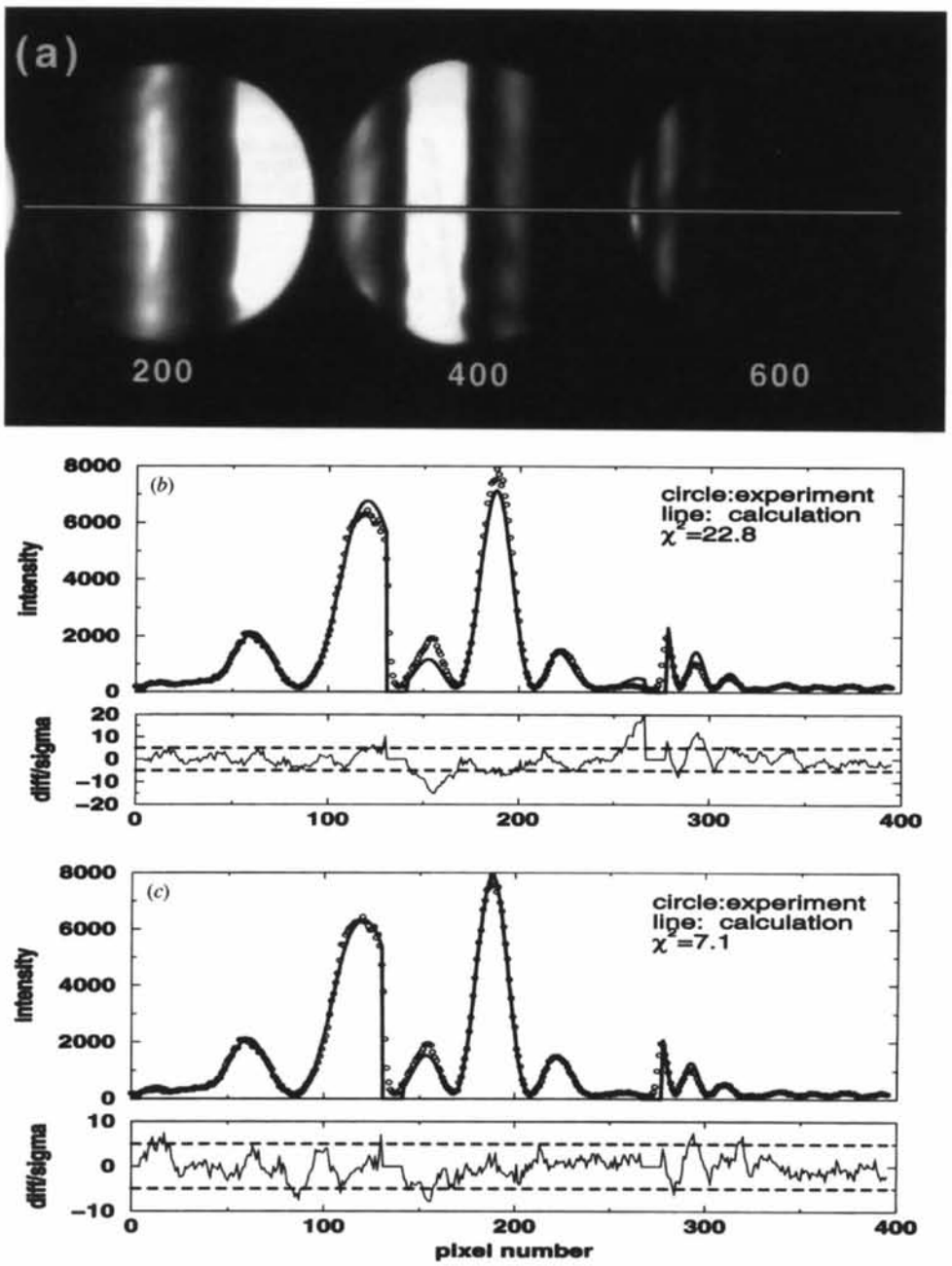

Fig. 4. (*a*) A CBED pattern of the (100) systematic row, where both 200 and 400 are in the Bragg condition. (*b*) A four-beam rocking-curve fit for determining U_{200} and U_{400}: $U_{200} = -0.012096$, $U_{400} = +0.014392\,\text{Å}^{-2}$, $t = 1527\,\text{Å}$; (*c*) 15-beam calculation refining U_{200} and U_{400}: $U_{200} = -0.011739$, $U_{400} = +0.016002\,\text{Å}^{-2}$, $t = 1529\,\text{Å}$.

necessary to improve U_{600} through further refinement by four-beam (000, 200, 400, 600) calculations. In these refinements, the U_{200} and the U_{400} were fixed as $U_{200} = -0.012\,22$, $U_{400} = +0.014\,38$ Å^{-2} and $U_{200} = +0.011\,05$, $U_{400} = +0.011\,93$ Å^{-2}, respectively, and $U_{600} = +0.016\,69$ Å^{-2} was used as the starting value in the refinements. It was found that the first set, *i.e.* $U_{200} = -0.012\,22$ and $U_{400} = +0.014\,38$ Å^{-2}, improved the rocking-curve fit of the $g600$ patterns, while the second set of the U_{200} and the U_{400} produced a

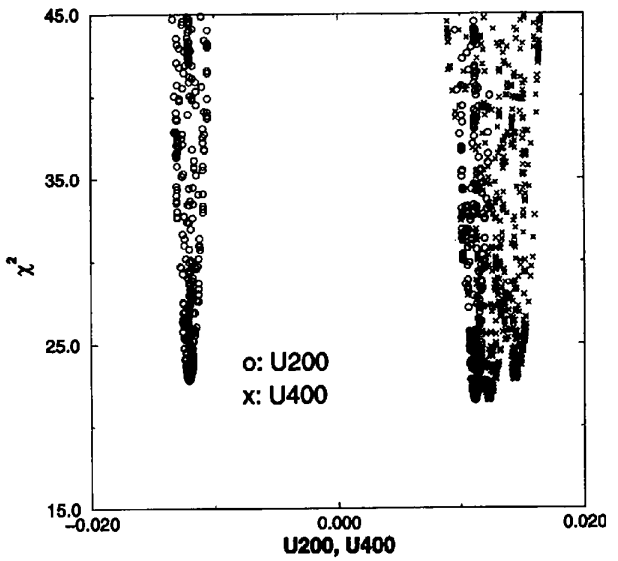

(*a*)

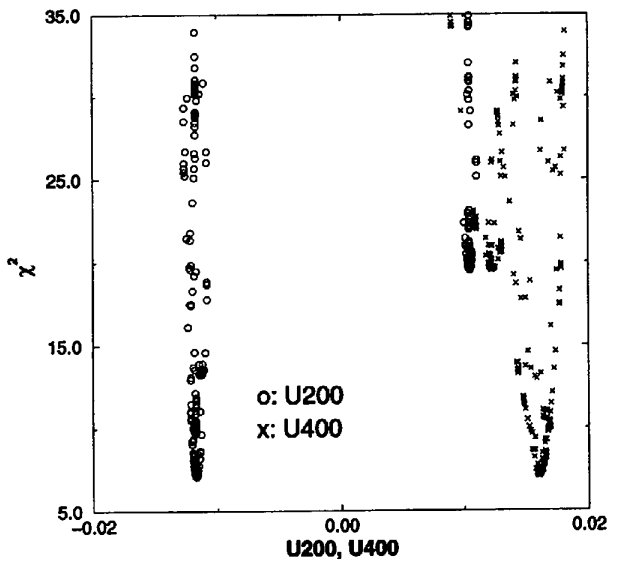

(*b*)

Fig. 5. (*a*) A plot of χ^2 as a function of U_{200}, U_{400} showing two local minima in a four-beam rocking-curve fit (corresponding to No. 2 in Table 2) with almost the same χ^2s. (*b*) The same relation showing that the local minima are distinguishable after using a 15-beam calculation (corresponding to Fig. 4*c*).

Table 3. *U_{600} refined by four-beam calculations*

(*a*) The values of $U_{200} = -0.012\,22$ and $U_{400} = +0.014\,38$ Å^{-2} were kept fixed.

No.	U_{600} (Å^{-2})	ΔU_{600} (Å^{-2})	t (Å)	χ^2
1	+0.013222	0.000046	1370	12.2
2	+0.014046	0.000049	1594	12.2
3	+0.013612	0.000075	1398	23.1
4	+0.014015	0.000096	1144	9.6
Average	+0.01372	0.00034		

(*b*) The values of $U_{200} = +0.011\,05$ and $U_{400} = +0.011\,93$ Å^{-2} were kept fixed.

No.	U_{600} (Å^{-2})	ΔU_{600} (Å^{-2})	t (Å)	χ^2
1	+0.018240	0.000067	1365	25.3
2	+0.019005	0.000063	1587	19.2
3	+0.018704	0.000089	1397	33.2
4	+0.018070	0.000116	1116	11.4
Average	+0.01850	0.00037		

fit that was actually worse than that of the two-beam calculation, see Table 3. Fig. 3(*c*) shows the improved rocking-curve fit of the CBED pattern in Fig. 3(*a*) based on a four-beam calculation. The χ^2 of this fitting is 12.2, which is better than 16.0 of the two-beam calculation, while the χ^2 for the second set was obtained as 25.3. The second set of U_{200} and U_{400} could therefore be excluded. The structure factor of $g600$ obtained from this second round of refinement is $U_{600} = +0.013\,72\,(34)$ Å^{-2}.

A number of $g800$–$g10,0,0$ CBED patterns were then recorded with the reflections 800 and 10,0,0 in the Bragg condition. Fig. 6(*a*) shows such a CBED pattern. The same procedure as for the U_{200}, U_{400} and U_{600} refinement was applied to the $g800$–$g10,0,0$ patterns. Since $U_g = U_{-g}$, an 11-beam (10,0,0, 800, ..., 000, ..., $\bar{8}00$, $\bar{1}0,0,0$) calculation was applied. The structure factor of the 200, 400 and 600 reflections obtained above were fixed in the calculation, while U_{800} and $U_{10,0,0}$ were refined from the rocking-curve fit. Since the structure factors of 12,0,0, 14,0,0, ..., 20,0,0 are not known at this step, only the first six beams could be included in the structure matrix and diagonalized while the other five beams were treated as perturbations by using the Bethe perturbation theory (see Spence & Zuo, 1992). It is safe to treat the reflections $\bar{2}00$, ..., $\bar{1}0,0,0$ as perturbations because when the reflections 800 and 10,0,0 are in the Bragg position the $\bar{2}00$ is already far away from its Bragg condition. Fig. 6(*b*) is an 11-beam rocking-curve fit of the CBED pattern shown in Fig. 6(*a*). Table 4 gives the U_{800} and $U_{10,0,0}$ refined from five different $g800$–$g10,0,0$ patterns. Besides the results given in Table 4, there is another local minimum which was found having almost the same χ^2 as the first one. Only after further refinement could the other local minimum be excluded. This will be discussed in detail in the following sections.

The same procedures for the structure-factor determination were applied to $g12,0,0$–$g14,0,0$ CBED

Table 4. *U_{800} and $U_{10,0,0}$ determined from 11-beam calculation*

No.	U_{800} (Å^{-2})	$U_{10,0,0}$ (Å^{-2})	t (Å)	χ^2
1	−0.005931	+0.003078	1505	19.4
2	−0.007819	+0.003858	1311	13.5
3	−0.007776	+0.003801	1341	10.2
4	−0.008310	+0.004208	711	11.1
5	−0.008368	+0.003917	621	24.6
Average	−0.00764 (89)	+0.00377 (37)		

patterns (Fig. 7*a*) with a 15-beam (14,0,0, 12,0,0, ..., 000, ..., $\bar{1}\bar{2}$,0,0, $\bar{1}\bar{4}$,0,0) calculation. As discussed by Taftø & Metzger (1985), the high-order reflections along a systematic row do not show many details in the rocking-curve fringes around the Bragg peaks. For the reflections with indices higher than 10,0,0, almost no rocking-curve fringes were observed besides the intensity peaks at their Bragg positions. This can be seen from both Fig. 6(*a*) and Fig. 7(*a*). Without the

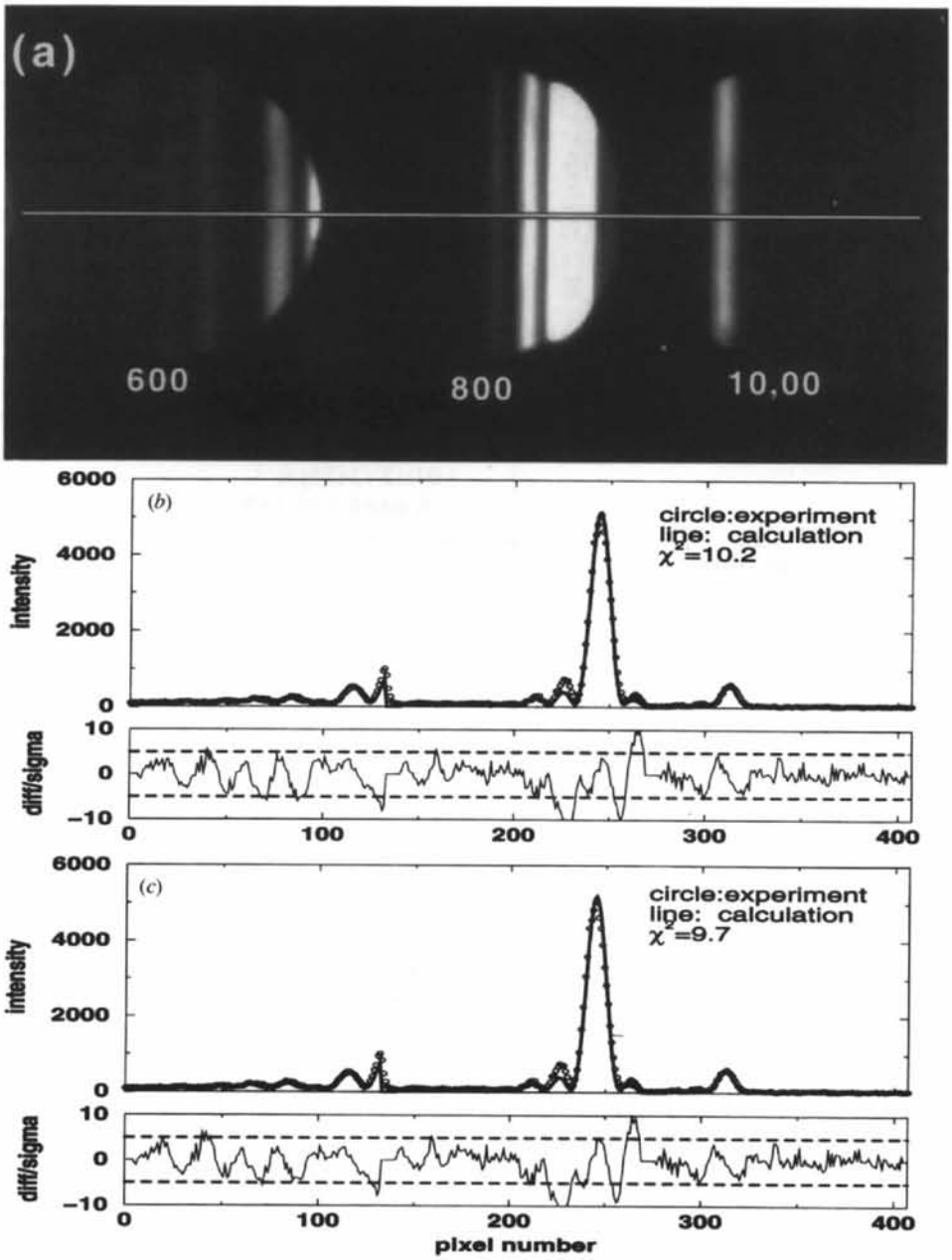

Fig. 6. (*a*) A CBED pattern of the (100) systematic row, where both $g800$ and $g10,0,0$ are in the Bragg condition. (*b*) 11-beam calculation for determining U_{800} and $U_{10,0,0}$: $U_{800} = -0.007\,776$, $U_{10,0,0} = +0.003\,801$ Å^{-2}, $t = 1341$ Å. (*c*) 15-beam refinement of U_{800} and $U_{10,0,0}$: $U_{800} = -0.006\,570$, $U_{10,0,0} = +0.003\,606$ Å^{-2}, $t = 1352$ Å.

rocking-curve fringes around the Bragg position, the thickness of the sample cannot be determined. Therefore, the fringes of the 800 reflection were included in the rocking-curve fit for determining the thickness although only the $U_{12,0,0}$ and $U_{14,0,0}$ were refined in the $g12,0,0$–$g14,0,0$ patterns. Fig. 7(*b*) shows a 15-beam rocking-curve fit. Table 5 gives the structure factors $U_{12,0,0}$ and $U_{14,0,0}$ determined from four different $g12,0,0$–$g14,0,0$ CBED patterns. Two different signs of $U_{14,0,0}$ were obtained from the rocking-curve fit with almost the same χ^2, while the amplitudes of the two $U_{14,0,0}$ are almost the same. It is difficult to obtain a

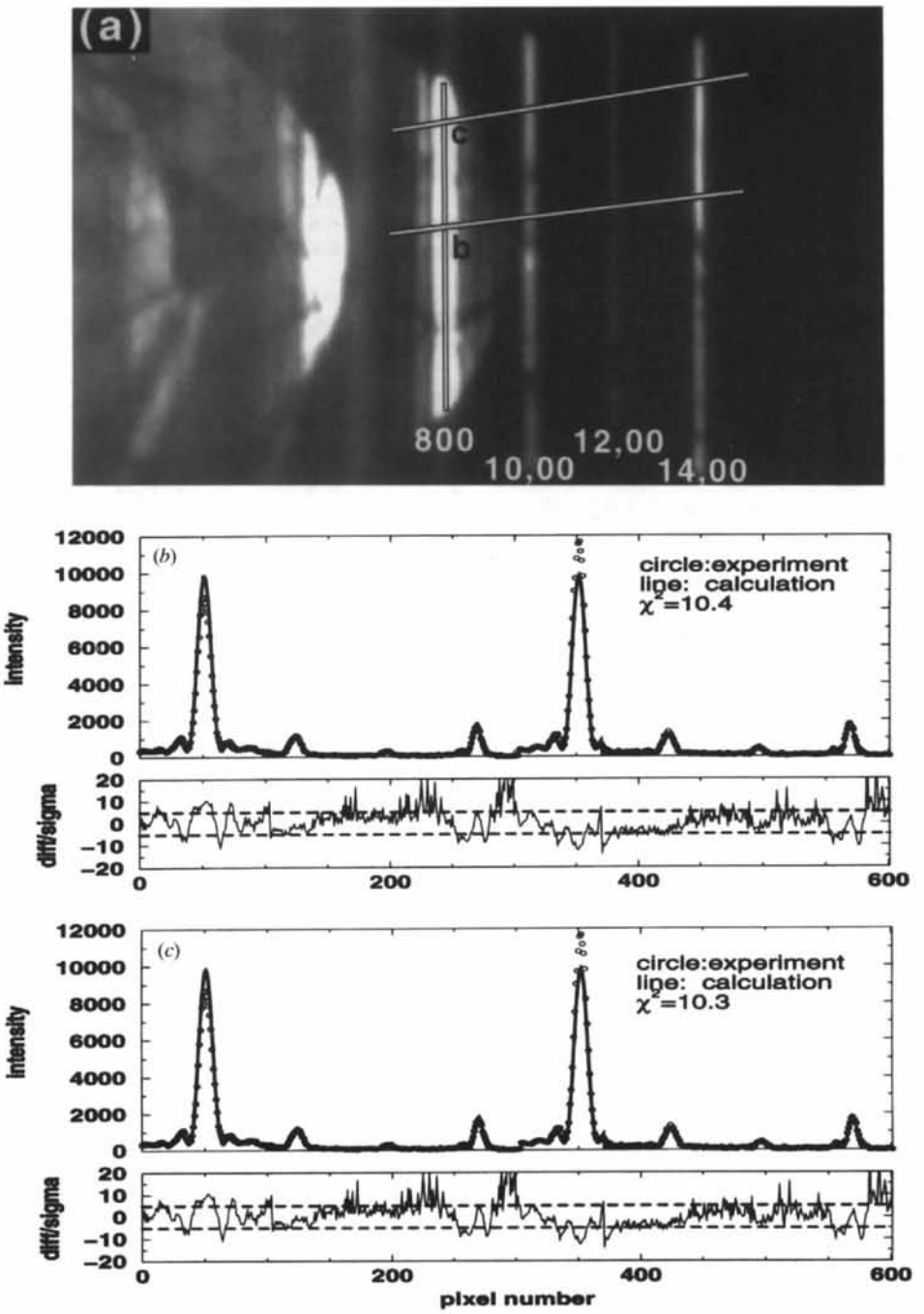

Fig. 7. (*a*) A CBED pattern of the (100) systematic row with a large convergent-beam angle. (*b*) 15-beam calculation for determining $U_{12,0,0}$ and $U_{14,0,0}$: $U_{12,0,0} = -0.001\,317$, $U_{14,0,0} = -0.002\,418\,\text{Å}^{-2}$, $t = 1366\,\text{Å}$. (*c*) 15-beam refinement of $U_{12,0,0}$ and $U_{14,0,0}$: $U_{12,0,0} = -0.001\,245$, $U_{14,0,0} = -0.002\,157\,\text{Å}^{-2}$, $t = 1376\,\text{Å}$.

Table 5. *$U_{12,0,0}$ and $U_{14,0,0}$ determined from 15-beam calculation*

No.	$U_{12,0,0}$ (Å^{-2})	$U_{14,0,0}$ (Å^{-2})	t (Å)	χ^2
1	−0.001739	−0.002855	1121	5.0
2	−0.001376	−0.002062	1511	22.1
3	−0.001455	−0.002041	1176	17.3
4	−0.001317	−0.002418	1366	10.4
5	−0.001177	−0.002571	711	12.4
Average	−0.00141 (19)	−0.00239 (31)		
No.	$U_{12,0,0}$ (Å^{-2})	$U_{14,0,0}$ (Å^{-2})	t (Å)	χ^2
1	−0.001523	+0.003112	1121	4.8
2	−0.001131	+0.001926	1511	21.8
3	−0.001215	+0.001894	1176	17.1
4	−0.001031	+0.002245	1376	10.1
5	−0.000897	+0.002402	711	11.9
Average	−0.00116 (21)	+0.00232 (44)		

distinct difference from the rocking-curve fit. When high-order reflections satisfy the Bragg condition, the excitation errors of all other reflections along the systematic row are very large except the one on the Bragg position. The weak dynamical effects of the high-order reflections makes the rocking-curve fit not very sensitive to the sign of the structure factors.

The next step was to repeat the structure-factor refinement iteratively using 15-beam ($\bar{1}4$,0,0, $\bar{1}2$,0,0, ..., 000, ..., 12,0,0, 14,0,0) calculations until there was no significant improvement of the χ^2 in the rocking-curve fit and no significant changes of the refined structure factors. Different beams were included in the scattering matrix for the different CBED patterns. For the $g200$–$g400$ patterns, for instance, eight beams ($\bar{4}00$, $\bar{2}00$, 000, 200, 400, 600, 800, 10,0,0) were included in the diagonalization, while the other seven reflections were treated as perturbation. For the $g600$ patterns, however, another set of eight beams ($\bar{2}00$, 000, 200, 400, 600, 800, 10,0,0, 12,0,0) was used in the diagonalization. Only the corresponding structure factors, *i.e.* the U_{200}, U_{400} for the $g200$–$g400$ patterns and U_{600} for the $g600$ patterns, were now refined while the other structure factors were fixed. 15-beam calculations improved the rocking-curve fit compared with the previous refinement, which involved less beams in the calculation. Fig. 3(*d*) shows a 15-beam refinement of U_{600} obtained by fitting the rocking curves of the 200, 400, 600 and 800 reflections. The χ^2 of this refinement is 17.6. Much more experimental data were included in this refinement than in the previous one. The refined structure factor is $U_{600} = +0.012\,884\,(54)$ Å^{-2} and the refined thickness is $t = 1330$ Å. Table 6 gives the U_{600} obtained from the 15-beam refinement of four $g600$ patterns. Fig. 4(*c*) is also a 15-beam rocking-curve fit of the CBED pattern in Fig. 4(*a*). The corresponding χ^2 is 7.1, which is much better than the χ^2 (22.8) of the four-beam calculation in Fig. 4(*b*). Table 7 gives U_{200} and U_{400} refined from six different $g200$–$g400$ CBED patterns. Fig. 6(*c*) and Fig.

Table 6. *U_{600} refined by 15-beam calculations*

No.	U_{600} (Å^{-2})	ΔU_{600} (Å^{-2})	t (Å)	χ^2
1	+0.012884	0.000054	1330	17.6
2	+0.012858	0.000044	1603	9.3
3	+0.012485	0.000061	1393	13.4
4	+0.012776	0.000103	1139	10.6
Average	+0.01275	0.00016		

Table 7. *U_{200} and U_{400} refined from 15-beam calculation*

No.	U_{200} (Å^{-2})	U_{400} (Å^{-2})	t (Å)	χ^2
1	−0.012104	+0.015770	1464	19.0
2	−0.011739	+0.016002	1529	7.1
3	−0.011492	+0.015173	1483	9.9
4	−0.012299	+0.015875	1206	10.7
5	−0.012236	+0.016686	1429	4.8
6	−0.011602	+0.016006	1728	12.1
Average	−0.01191 (31)	+0.01592 (44)		

Table 8. *U_{800} and $U_{10,0,0}$ refined from 15-beam calculations*

No.	U_{800} (Å^{-2})	$U_{10,0,0}$ (Å^{-2})	t (Å)	χ^2
1	−0.005179	+0.002989	1520	18.8
2	−0.006600	+0.003639	1316	13.9
3	−0.006570	+0.003606	1352	9.7
4	−0.007070	+0.003985	711	11.9
5	−0.007220	+0.003736	621	26.2
Average	−0.00653 (72)	+0.00359 (33)		

Table 9. *$U_{12,0,0}$ and $U_{14,0,0}$ refined from 15-beam calculation*

No.	$U_{12,0,0}$ (Å^{-2})	$U_{14,0,0}$ (Å^{-2})	t (Å)	χ^2
1	−0.001675	−0.002644	1121	5.3
2	−0.001308	−0.001845	1526	22.2
3	−0.001367	−0.001805	1176	17.0
4	−0.001245	−0.002157	1376	10.3
5	−0.001134	−0.002267	711	13.4
Average	−0.00135 (18)	−0.00214 (31)		
No.	$U_{12,0,0}$ (Å^{-2})	$U_{14,0,0}$ (Å^{-2})	t (Å)	χ^2
1	−0.001487	+0.003041	1121	4.9
2	−0.001087	+0.001845	1526	21.9
3	−0.001158	+0.001778	1181	17.1
4	−0.000992	+0.002113	1386	10.1
5	−0.000890	+0.002232	711	13.3
Average	−0.00112 (20)	+0.00220 (45)		

Table 10. *Measured structure factors of reflections along the (100) systematic row*

h00	U_g (Å^{-2})
200	−0.01191 (31)
400	+0.01592 (44)
600	+0.01275 (16)
800	−0.00653 (72)
10,0,0	+0.00359 (33)
12,0,0	−0.00135 (18)
14,0,0	−0.00214 (31)
or	
12,0,0	−0.00112 (20)
14,0,0	+0.00220 (45)

7(*c*) are the rocking-curve fits of the 15-beam structure-factor refinement of U_{800}, $U_{10,0,0}$, $U_{12,0,0}$ and $U_{14,0,0}$, respectively. The refinement results are given in Tables 8 and 9. Table 10 gives all the structure-factor amplitudes and signs of the reflections along the (100) systematic row determined by a quantitative rocking-curve fit.

4. Discussion

4.1. *Local minima in the structure-factor refinement*

The global refinement procedure (Nüchter *et al.*, 1995) was used in the structure-factor determination. This is necessary because several parameters were refined simultaneously and no previous knowledge about the structure factors was available. As discussed in §2.3, the three geometrical parameters can be determined accurately from the refinement. Also, if enough rocking-curve fringes are seen in the CBED patterns, the thickness of the illuminated sample area can be determined accurately. The different local minima in the refinement are, therefore, mainly caused by different choices of the structure-factor amplitudes or signs. The best rocking-curve fit or the smallest χ^2 should correspond to the correct structure factors in the refinement. However, in some cases, a number of local minima have almost the same χ^2s, the difference between them being too small to decide which one is the correct structure factor. In some of the cases, more beams have to be included in the calculation in order to distinguish between the different local minima. An example is the four-beam refinement of U_{200} and U_{400}. Typically, two local minima corresponding to different sign combinations of U_{200} and U_{400} were found in the rocking-curve fit (Fig. 5*a*). Only when more beams are included in the refinement does the χ^2 difference between the two local minima become big enough to select the right structure factors. Fig. 5(*b*) shows the same two local minima as in Fig. 5(*a*), but with a 15-beam calculation. From the difference in the χ^2s of these two local minima, one is now able to tell which one corresponds to the correct structure factors. Fig. 4(*c*) is the best rocking-curve fit using a 15-beam calculation with a χ^2 of 7.1.

For the higher-order reflections, the difference of the χ^2s of the local minima is often even smaller than in the lower-order case. For instance, the refinement of $U_{10,0,0}$ from $g800$–$g10,0,0$ CBED patterns, where many beams are already included in the refinements, yields two different values of $U_{10,0,0}$ with almost the same χ^2. Only after iterating the refinement of all the structure factors with 15-beam calculations several times does the difference of the χ^2s become sufficiently large to exclude one of the local minima.

However, when the dynamical interaction along the systematic row becomes very weak, the rocking-curve fitting for the high-order reflections may no longer be sensitive to the sign of the corresponding structure factors. Two local minima can then no longer be distinguished from the difference of the χ^2s. Two results corresponding to different signs of $U_{14,0,0}$ are shown in Tables 5 and 9 as an example where the difference of the χ^2s is too small to tell which one should corresponding to the correct structure factor. (The structure factors of all other reflections given in Table 10 correspond to the negative sign of $U_{14,0,0}$.) Since the main difference of the two results is only the sign of $U_{14,0,0}$, one possible way to distinguish them is by estimating its probability by using the statistical method proposed by Woolfson (1961) along the systematic row.

4.2. *Definition of the unit-cell origin*

The diffracted intensities and hence the structure-factor amplitudes of the different reflections are independent of the choice of origin. However, the phases of the structure factors will depend on the position of the origin. The space group with the corresponding set of symmetry operators already imposes some restrictions on the choice of origin. Only the sites with the same point symmetry will be suitable and represent the so-called permissible origins, among which the origin has to be chosen. This may be done by fixing the signs of a limited number of suitable structure factors. In the present centrosymmetric case of the body-centered tetragon, the phases of the reflections in the $h00$ row can be chosen as either 0 or π. The origin will then be fixed by the choice of sign of one structure factor in the row. Here, the sign of U_{600} was set as positive. If the sign of this structure factor was chosen as negative, it would change the signs of all structure factors $h00$, where $h = 4n + 2$, to the opposite sign, while the signs of other reflections would be unchanged (see, for instance, Giacovazzo, 1992). The intensity profiles of the rocking curves will of course be the same.

4.3. *Accuracy of the measurement*

The error analysis of the structure-factor refinement was discussed in detail by Spence (1993). The standard deviations of U_{600} measured from each single CBED pattern are given in Tables 1, 3 and 6. The error of the averaged structure factors results, however, mainly from the dynamical interaction of the off-systematic reflections with the systematic reflections, which is much larger than the errors of each single refinement.

The excitation of the off-systematic reflections is always unavoidable, which will affect the intensity distribution inside the diffraction discs. Hence, the intensity distribution *parallel* to the rocking-curve fringes is not uniform. Fig. 8(*a*) shows such an

intensity profile, which was obtained from a line scan along the Bragg peak of the 800 reflection [indicated as a vertical line in Fig. 7(*a*)]. The intensities of this profile in regions *b* and *c*, which correspond to the *b* and *c* in Fig. 7(*a*), are different. Therefore, the two other line scans in Fig. 7(*a*) across the 800 reflection from regions marked *b* and *c* give different intensity distributions around the Bragg position of the 800 reflection (see Figs. 7*b* and *c*). For a completely unknown structure like Al_mFe, we do not know how to correct for the influence of the off-systematic reflections since the corresponding structure factors are not known. Because of the dynamical effects, the rocking curves of the 800 reflection have to be included as a reference in the refinement of $U_{12,0,0}$ and $U_{14,0,0}$. When the two rocking curves were fit separately, the χ^2 of the two fits are almost the same but the structure factors refined from each fit are different. Figs. 8(*b*) and (*c*) show the fits of two rocking curves, corresponding to the line scans *b* and *c* marked in Fig. 7(*a*), obtained by 15-beam calculations. The structure factors refined in Fig. 8(*b*) are $U_{12,0,0} = -0.001\,252\,(69)$, $U_{14,0,0} = -0.002\,253\,(46)\,\text{Å}^{-2}$ and $\chi^2 = 6.5$; while those refined from Fig. 8(*c*) are: $U_{12,0,0} = -0.001\,242\,(55)$, $U_{14,0,0} = -0.002\,042\,(37)\,\text{Å}^{-2}$ and $\chi^2 = 6.2$. If two rocking curves are fit together (Fig. 7*c*), which leads

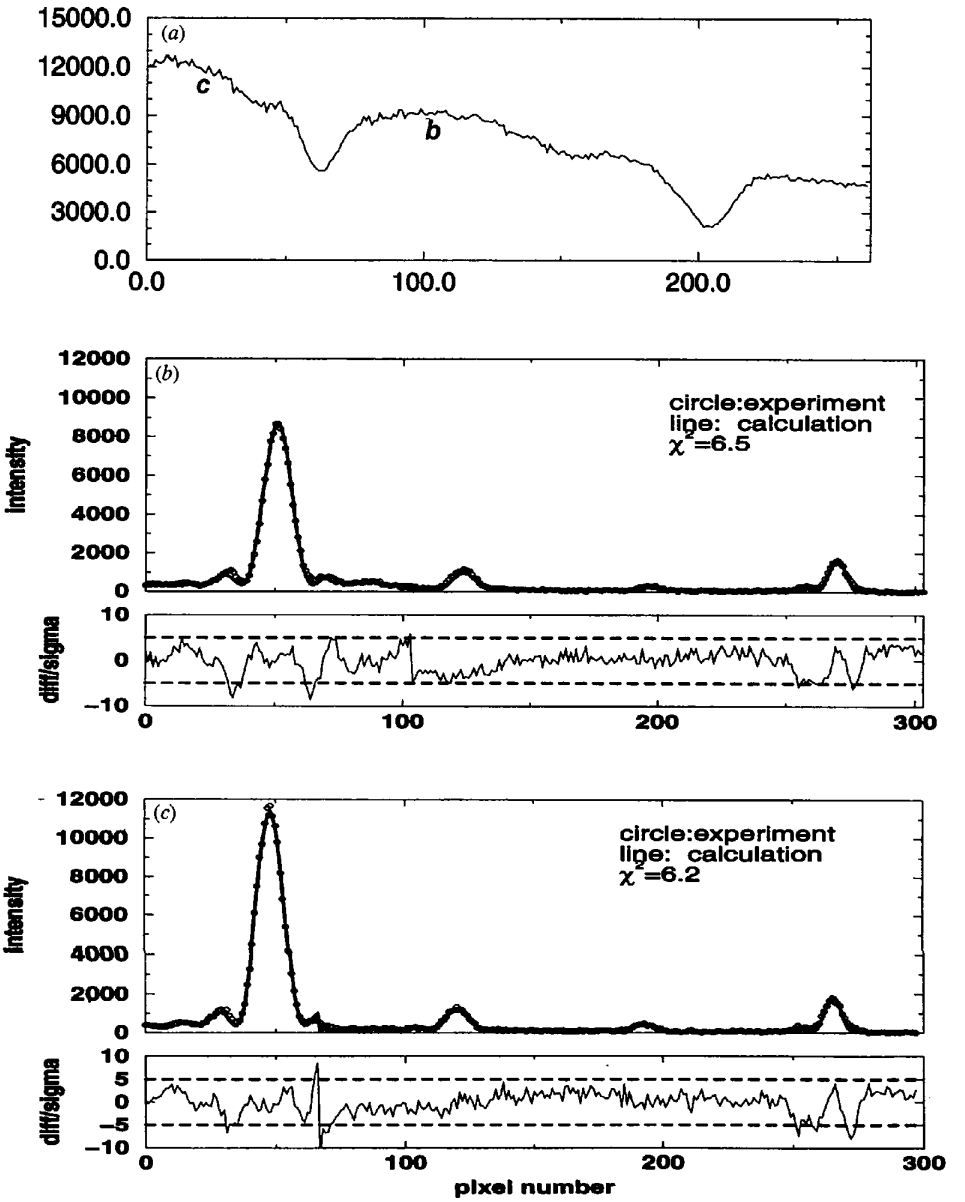

Fig. 8. (*a*) An intensity profile taken from the CBED pattern shown in Fig. 7(*a*) where the vertical line indicated the position of the line scan. (*b*) and (*c*) are 15-beam fits of two rocking curves that are obtained from the line scans *b* and *c* in Fig. 7(*a*) separately.

to a higher χ^2 (10.3) than two individual fits, the refined structure factors [$U_{12,0,0} = -0.001\,245\,(56)$ Å^{-2}, $U_{14,0,0} = -0.002\,157\,(37)$ Å^{-2}] are the averages of the structure factors refined from two separated rocking-curve fits in Figs. 8(*b*) and (*c*).

The intensity of the rocking curve around the Bragg positions could be changed by tilting the crystal to another orientation around the same systematic row because of the dynamical interaction of different off-systematic row reflections. Therefore, for a completely unknown phase, even if the rocking curve obtained from one CBED pattern could be fitted very well (χ^2 is smaller than 5, for instance), it does not mean that the right structure factor has been obtained. It is important to fit a number of rocking curves of different CBED patterns acquired from different orientations and different thicknesses of the crystal. If the structure factors refined from those CBED patterns agree within reasonable error ranges, it is most likely that the correct structure factors are found. Table 10 gives the structure factors and their standard deviations for the reflections from 200 up to 14,0,0.

However, the error caused by the limited number of beams involved in the refinement could not be excluded by averaging the structure factors refined from different diffraction conditions. This error could only be excluded by increasing the number of beams included in the refinement along the systematic row and repeating the iterative procedure until a stable result is obtained. This means that at the beginning of the iterative procedure the deviation of the refined structure factor from the final result could be much larger than the error bar given from averaging in each individual step. U_{600} shown in Tables 1, 3 and 6 is an example where the deviation of $|U_{600}| = 0.016\,69\,(28)$ in Table 1 from the final result of $|U_{600}| = 0.012\,75\,(16)$ in Table 6 is much larger than its error bar. Even so, it is still important to estimate the error bar of the refined structure factors at each step of the iterative procedure, even at the beginning stages, because it confirms that the refined structure factors could be used for further refinement.

Since we have applied this quantitative CBED technique to an unknown structure for the first time, it is rather difficult to give a very detailed error analysis, in particular of the systematic errors. A detailed identification and quantification of possible systematic errors of this new method definitely requires more experience and more work on a number of different systems.

4.4. *Absorption*

In the iterative refinement procedure described above, we did not account for absorption in the many-beam calculation. However, for some test cases, we did include it in the calculation. For the CBED patterns of the low-order reflections, such as *g*200–*g*400 and *g*600 patterns, the χ^2s of the rocking-curve fits decreased significantly when absorption was included in the refinement. The refined structure factors remained inside the error bars of those refined without the absorption. However, different refinement results for the absorption potential were obtained from the rocking-curve fitting of different CBED patterns. The error bars of the averaged absorption potentials from different CBED patterns are much larger than those of the corresponding structure factors. As discussed in §4.3, the goodness of the rocking-curve fit is affected by the excitation of off-systematic reflections. When absorption is included in the refinement, it compensates for the ignored off-systematic reflections, which explains the quite different absorption potentials refined from different CBED patterns. Since these absorption potentials are physically not correct, we decided not to treat the effect of absorption in the refinement. It is difficult to know if there is any systematic error caused by ignoring the absorption, but our results show that the structure factors refined together with absorption is inside the error bar of the structure factors refined without absorption.

5. Concluding remarks

The motivation of the present research has been to determine structure-factor amplitudes, and their phases, for use in *ab initio* structure determination by electron diffraction techniques. It is shown here that the structure factor for an unknown structure can be determined by an iterative procedure for reflections in a systematic row. The sign determination depends on multiple-beam interactions along the row. However, the present iterative procedure will become tedious if a large number of reflections are needed. It is not a practical alternative to obtain a complete data set from this method. But, on the other hand, such accurate structure-factor data cannot be obtained, so far, by any other electron diffraction technique. The main application may therefore be a combination of this method with other techniques that can yield larger sets of intensity data, especially if these data can be treated as near-kinematical.

From the crystallographic viewpoint, a correct structure could be revealed using the method of Fourier synthesis with the knowledge of correct phases and amplitudes of low-order reflections together with the more or less correct phases and amplitudes of high-order reflections (Peng & Wang, 1994). The quantitative CBED could provide a part of the data, *i.e.* correct phases and amplitudes of low-order reflections, and also part of the high-order reflections. Precession electron diffraction is another alternative to provide near-kinematical amplitudes of high-order reflections. The signs or phases obtained

by the present method can then be introduced as input for phase determination by other procedures like the direct phasing method. In a further study of the structure of Al_mFe (Gjønnes, Hansen, Berg, Midgley & Cheng, 1995), the structure-factor signs obtained here have been used as a check on models used for Fourier calculations.

In summary, in this paper, we have shown a successful example of applying quantitative CBED to a crystal of completely unknown structure by using an iterative method for determination of accurate structure-factor amplitudes and signs. The main advantage of this method is that it is the only one that is able to deal with the dynamical scattering effects of crystals of unknown structures. Therefore, it provides the structure-factor amplitudes and signs with very high accuracy for the *ab initio* structure determination. In this work, we have chosen a centrosymmetric projection where the phases of the structure factors are either 0 or π. The same iterative method could also be applied to non-centrosymmetric projections for determining the accurate amplitudes and phases of the structure factors.

YFC is grateful to the Alexander von Humboldt Foundation for an AvH Research Fellowship. Bjørn S. Berg provided the powder samples of Al_mFe. YFC also thanks Professor F. H. Li for many stimulating discussions and for her encouragement. Part of the work was supported by the Stiftung Volkswagenwerk under contract I/68313.

References

Bird, D. M. & Saunders, M. (1992). *Acta Cryst.* A**48**, 555–562.

Cheng, Y. F., Hui, M. J. & Li, F. H. (1991). *Philos. Mag. Lett.* **63**, 49–55.

Deininger, C., Necker, G. & Mayer, J. (1994). *Ultramicroscopy*, **54**, 15–30.

Dorset, D. L. (1991). *Ultramicroscopy*, **38**, 23–40.

Giacovazzo, C. (1992). *Fundamentals of Crystallography*. Oxford University Press.

Gjønnes, J., Hansen, H., Berg, B. S., Midgley, P. A. & Cheng, Y. F. (1995). *Inst. Phys. Conf. Ser.* No. 147, Section 4, pp. 121–124.

Hansen, V., Berg, B. S. & Gjønnes, J. (1995). Personal communication.

Holmestad, R., Zuo, J. M., Spence, J. C. H., Høier, R. & Horita, Z. (1995). *Philos. Mag.* A**72**, 579–601.

Ma, Y., Romming, C., Lebech, B., Gjønnes, J. & Taftø, J. (1992). *Acta Cryst.* B**48**, 11–19.

Midgley, P. A., Sleight, M. E. & Vincent, R. (1994). Proc. 12th International Congress on Electron Microscopy, Paris, Vol. 1, pp. 919–920.

Miki, I., Kosuge, H. & Nagahama, K. (1975). *J. Jpn Inst. Met.* **25**(1), 1–9.

Nüchter, W., Weickenmeier, A. & Mayer, J. (1995). Unpublished.

Peng, L. M. & Wang, S. Q. (1994). *Acta Cryst.* A**50**, 759–771.

Simensen, C. J., Fartum, P. & Anderson, A. (1984). *Fresenius Z. Anal. Chem.* **319**, 286–292.

Skjerpe, P. (1988). *Acta Cryst.* B**44**, 480–486.

Skjerpe, P., Gjønnes, J. & Langsrud, Y. (1987). *Ultramicroscopy*, **22**, 239–250.

Spence, J. C. H. (1993). *Acta Cryst.* A**49**, 231–260.

Spence, J. C. H. & Zuo, J. M. (1992). *Electron Microdiffraction*. New York: Plenum Press.

Strid, J. & Simensen, C. J. (1986). *Prac. Metal.* **23**, 485–492.

Taftø, J. & Metzger, T. H. (1985). *J. Appl. Cryst.* **18**, 110–113.

Vincent, R. & Bird, D. M. (1986). *Philos. Mag.* A**53**, L35–L40.

Vincent, R. & Exelby, D. R. (1995). *Acta Cryst.* A**51**, 801–809.

Vincent, R. & Midgley, P. A. (1994). *Ultramicroscopy*, **53**, 271–282.

Weickenmeier, A., Nüchter, W. & Mayer, J. (1995). *Optik (Stuttgart)*, **99**, No. 4, 147–154.

Woolfson, M. M. (1961). *Direct Methods in Crystallography*. Oxford: Clarendon Press.

Zuo, J. M. & Spence, J. C. H. (1991). *Ultramicroscopy*, **35**, 185–196.

Zuo, J. M., Spence, J. C. H. & O'Keeffe, M. (1988). *Phys. Rev. Lett.* **61**, 353–356.